Author/s:
Darwinkel, A;Stanić, D;Booth, LC;May, CN;Lawrence, AJ;Yao, ST

Title:
Distribution of orexin-1 receptor-green fluorescent protein- (OX1-GFP) expressing neurons in the mouse brain stem and pons: Co-localization with tyrosine hydroxylase and neuronal nitric oxide synthase

Date:
2014-01-01

Citation:
Darwinkel, A., Stanić, D., Booth, L. C., May, C. N., Lawrence, A. J. & Yao, S. T. (2014). Distribution of orexin-1 receptor-green fluorescent protein- (OX1-GFP) expressing neurons in the mouse brain stem and pons: Co-localization with tyrosine hydroxylase and neuronal nitric oxide synthase. Neuroscience, 278 (1), pp.253-264. https://doi.org/10.1016/j.neuroscience.2014.08.027.

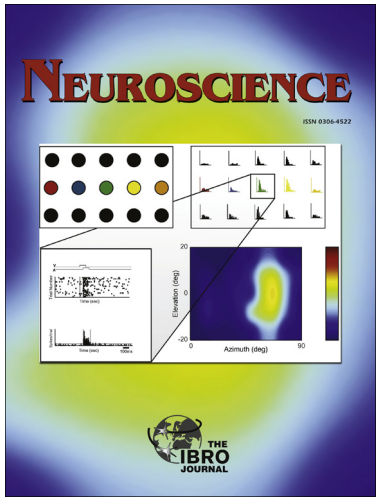

Distribution of orexin-1 receptor-green fluorescent protein- (OX_1-GFP) expressing neurons in the mouse brain stem and pons: co-localisation with tyrosine hydroxylase and neuronal nitric oxide synthase

Amber Darwinkel, Davor Stanić, Lindsea C. Booth, Clive N. May, Andrew J. Lawrence, Song T. Yao

PII: S0306-4522(14)00704-0
DOI: http://dx.doi.org/10.1016/j.neuroscience.2014.08.027
Reference: NSC 15646

To appear in: *Neuroscience*

Accepted Date: 14 August 2014

Please cite this article as: A. Darwinkel, D. Stanić, L.C. Booth, C.N. May, A.J. Lawrence, S.T. Yao, Distribution of orexin-1 receptor-green fluorescent protein- (OX_1-GFP) expressing neurons in the mouse brain stem and pons: co-localisation with tyrosine hydroxylase and neuronal nitric oxide synthase, *Neuroscience* (2014), doi: http://dx.doi.org/10.1016/j.neuroscience.2014.08.027

Distribution of orexin-1 receptor-green fluorescent protein- (OX_1-GFP) expressing neurons in the mouse brain stem and pons: co-localisation with tyrosine hydroxylase and neuronal nitric oxide synthase.

Amber Darwinkel, Davor Stanić, Lindsea C. Booth, Clive N. May, Andrew J. Lawrence and Song T. Yao*

Florey Institute of Neuroscience and Mental Health, Howard Florey Laboratories, Royal Parade, University of Melbourne, VIC 3010, Australia

*Correspondence:

Song T. Yao

The Florey Institute of Neuroscience and Mental Health

Howard Florey Laboratories

Royal Parade,

University of Melbourne, VIC 3010

T: +61 3 8344 0182

F: +61 3 9348 1707

E: song.yao@florey.edu.au

Running Title: Brainstem distribution of OX_1 receptors

Key words: Orexin, receptor, immunohistochemistry, medulla oblongata, green fluorescent protein

ABBREVIATIONS:

10N	Dorsal motor nucleus of the vagus
12N	hypoglossal nucleus
A5	A5 noradrenergic cell group
Amb	Nucleus ambiguus
AP	Area postrema
BAC	Bacterial artificial chromosome
BIC	Nucleus of the brachium of the inferior colliculus
Cu	Cuneate nucleus
DLPAG	Dorsolateral periaqueductal grey
DMPAG	Dorsomedial periaqueductal grey
DRD	Dorsal raphe nucleus, dorsal part
DRI	Dorsal raphe nucleus, infascicular part
DRN	Dorsal raphe nucleus
DRVL	Dorsal raphe nucleus, ventrolateral part
ECIC(2)	External cortex of the inferior colliculus
GFP	Green Fluorescent Protein
GiV	Gigantocellular reticular nucleus
Gr	Gracile nucleus
IS	Inferior salivatory nucleus
LC	Locus coeruleus
LDTg	Laterodorsal tegmental nucleus
LPAG	Lateral periaqueductal grey
LPGi	Lateral paragigantocellular nucleus
MnR	Median Raphe nucleus
Mo5	Motor trigeminal nucleus
mRNA	Messenger ribose nucleic acid
MVePC	Medial vestibular nucleus, parvicellular part
MVeMC	Medial vestibular nucleus, magnocellular part
MVe	Medial vestibular nucleus
NOS1	Nitric oxide synthase, type 1
NTS	Nucleus of the solitary tract
OX_1	Orexin-1 receptor subtype
OX_2	Orexin-2 receptor subtype
PBS	Phosphate buffered saline
PCRtA	Parvicellular reticular nucleus
PFA	Paraformaldehyde
PMn	Paramedian reticular nucleus
PnR	Pontine raphe nucleus
PPTg	Pedunculopontine tegmental nucleus
RMg	Raphe magnus nucleus
ROb	Raphe obscurus nucleus
RtTg	Reticulotegmental nucleus of the pons
RPa	Raphe pallidus nucleus
RVLM	Rostral ventrolateral medulla
SolIM	Nucleus of solitary tract, intermediate part
Sp5C	Spinal trigeminal nucleus, caudal
SubCD	Nucleus sub-coeruleus
TH	Tyrosine hydroxylase

ABSTRACT

We used a reporter mouse line in which green fluorescent protein (GFP) was inserted into the orexin-1 receptor (OX_1) locus to systematically map the neuroanatomical distribution of the OX_1 receptor in the mouse brainstem and pons. Here, we show that the OX_1 receptor is expressed in a select subset of medullary and pontine nuclei. In the medulla, we observed OX_1-GFP expression in the cuneate, gracile, dorsal motor nucleus of the vagus (10N), nucleus of the solitary tract and medullary raphe areas. In the pons, the greatest expression was found in the locus coeruleus (LC) and dorsal raphe nucleus (DRN). High to moderate expression was found in the pedunculopontine tegmental nucleus (PPTg), laterodorsal tegmental nucleus, A5 cell group and the periaqueductal grey. Double-labelling with neuronal nitric oxide synthase (NOS1) revealed extensive co-localisation in cell bodies and fibres of the dorsal motor nucleus of the vagus, A5 cell group and the pedunculopontine tegmental nucleus. Double-staining with tyrosine hydroxylase (TH) revealed extensive co-expression in the LC, DRN and the lateral paragigantocellularis cell group in the ventral medulla. Our findings faithfully recapitulate the findings of OX_1 mRNA expression previously reported. This is the first study to systematically map the neuroanatomical distribution of OX_1 receptors within the mouse hindbrain and suggests that this OX_1-GFP transgenic reporter mouse line might be a useful tool with which to study the neuroanatomy and physiology of OX_1 receptor expressing cells.

Introduction

The neuropeptides Orexin-A and Orexin-B are produced via the proteolytic cleavage of a 130 amino acid long prepro-orexin protein, coded by a single gene transcript into 33 and 28 amino acid peptides, respectively (Sakurai et al., 1998). The prepro-orexin gene and protein are expressed by subsets of neurons located around the fornix, lateral hypothalamic area and dorsomedial hypothalamus. While the distribution of these neurons is localised within the hypothalamus, they have widespread projections that extend throughout the central nervous system (Peyron et al., 1998; Date et al., 1999). Unsurprisingly, the orexinergic system has been implicated in a range of diverse functions including the control of the sleep-wake cycle (Inutsuka & Yamanaka, 2013; Xu et al., 2013), thermoregulation (Tupone et al., 2011), feeding (Kay et al., 2014), reward (Lawrence 2010; Xu et al., 2013), and neuroendocrine (Inutsuka & Yamanaka, 2013) and cardiovascular regulation (Antunes et al., 2001; Carrive, 2013; Ciriello et al., 2013).

The actions of both orexin-A and orexin-B are mediated by two different G-protein coupled receptors: orexin-1 (OX_1) and orexin-2 (OX_2) (Sakurai et al., 1998). Pharmacological studies demonstrate that both orexin-A and orexin-B have similar affinities for OX_2 receptors, whereas orexin-A is 10-fold more selective for OX_1 receptors than orexin-B (Sakurai et al., 1998). As such, orexin-A is widely regarded as being selective for OX_1 receptors. Activation of OX_1 receptors within the ventrolateral periaqueductal grey has been shown to induce anti-nociception (Ho et al., 2011), while in the hindbrain, OX_1 receptors modulate meal size (Parise et al., 2011). In the rostral ventrolateral medulla (RVLM), OX_1 receptors have been suggested to be expressed on sympathoexcitatory bulbospinal neurons as exogenous application of orexin-A has been shown to elicits increases in blood pressure, sympathoexcitation and increases baroreflex sensitivity (Shahid et al., 2012).

There have been few studies that have mapped the distribution of the OX_1 and OX_2 receptor subtypes within the mammalian brain. There have, however, been comprehensive studies

describing the distribution of the OX_1 receptor messenger RNA (Marcus et al., 2001; Hervieu et al., 2001). This is most likely due to the fact that producing specific antibodies to G-protein coupled receptors has been challenging. Many of the available antibodies appear to lack specificity and produce high levels of background staining. To circumvent this issue, we used an enhanced green fluorescent protein (GFP) reporter mouse to characterise the distribution of OX_1 receptors within the mouse brain stem and pons. Additionally, given the evidence for interactions between the orexinergic, nitrergic (Shih and Chuang, 2001; Xiao et al., 2013) and catecholaminergic (Soya et al., 2013; Shahid et al., 2012) systems, we also performed a systematic analysis of OX_1-GFP co-localisation with the neuronal isoform of nitric oxide synthase (NOS1) and a synthetic enzyme for catecholamines, tyrosine hydroxylase (TH).

Methods

All experimental protocols used in this study were performed in accordance with the Prevention of Cruelty to Animals Act, Australia 1986, conformed with the guidelines set out by the National Health and Medical Research Council of Australia (2007), and were approved by the Florey Institute of Neuroscience and Mental Health Animal Ethics Committee.

To determine the distribution of OX_1 receptors in the brainstem and pons, adult male transgenic OX_1-GFP (BAC) reporter mice (founder line KP68Gsat/Mmed) from the Mutant Mouse Regional Resource Centers on a CD-1 background were used (n=8). A GFP reporter gene, followed by a polyadenylation sequence, was inserted into BAC clone RP23-282L14 at the initiating ATG codon of the first coding exon of the Hcrtr1 gene. The modified BAC containing the inserted GFP upstream of the Hcrtr1 gene was injected into the pronuclei of FVB/N fertilized oocytes. Hemizygous progeny were mated to Crl:CD1(ICR) mice. The original founder animals were a gift from Dr Danny Winder (Vanderbilt University, Nashville, TN) and Dr Paul Kenny (Mount Sinai School of Medicine, New York, NY). All mice used in this study were males aged between 18-22 weeks. Mice were housed under 12h-12h light-dark conditions and allowed *ad libitum* access to standard laboratory chow (Barastoc, Australia) and tap water.

Perfusion

All perfusions were performed during the light phase (between 9:00-12:00). Mice (35-42 g) were deeply anaesthetised with sodium pentobarbitone (100 mg/kg i.p.), and perfused with 50 ml of 0.1 M phosphate buffered saline (PBS; pH 7.4) at 90-120 mmHg of perfusion pressure followed by 50 ml of 4% paraformaldehyde (PFA; w/v; Merck Millipore). The brain was then removed and transferred to 4% PFA for 4 hours then PBS containing 20% sucrose (w/v) and stored at 4℃ until processed.

Prior to sectioning, the brains were frozen over liquid nitrogen and four sets of coronal sections were cut (30 µm thickness) on a cryostat (Leica Cryocut 1850, Leica Microsystems, Wetzlar, Germany). The free-floating sections were collected in 24-well tissue culture plates containing PBS prior to being processed for immunohistochemical detection of GFP, NOS1 and TH.

Immunohistochemical detection of GFP

For immunohistochemical detection of GFP, we used a commercial chicken polyclonal GFP antisera directed against the full-length recombinant GFP protein (Abcam, Cambridge, UK; catalogue number: ab13970, lot number: 13879-5). The specificity of this antibody has been extensively characterised in the past and has been shown to be highly specific (Llewellyn-Smith et al., 2011; Leinders-Zufall et al., 2014). Immunohistochemistry was performed as described previously (Yao et al., 2012). Free-floating mouse brain stem sections were incubated for 10 minutes in a blocking solution comprising 10% normal goat serum (NGS, Sigma-Aldrich, MO) and 0.3% Triton X-100 (Sigma-Aldrich) in 0.1 M PBS followed by rinses in PBS (3 x 10 minutes). Sections were then incubated in a polyclonal chicken anti-GFP primary antiserum (1:10,000 dilution) in PBS containing 0.3% Triton X-100 for 24 hours at 4°C. After the primary antibody incubation, sections were rinsed in PBS (3 x 10 minutes) prior to a 1 hour incubation in PBS containing biotinylated goat anti-chicken IgG (1:500 dilution, Jackson Laboratories, PA, USA), in PBS/0.3% Triton X-100 at room temperature. Following rinses in PBS (3 x 10 minutes), the sections were incubated for 1 hour in streptavidin-conjugated Alexfluor-488 (1:500 dilution, Life Technologies, UK) in PBS containing 0.3% Triton X-100. Subsequent to further washes (3 x 10 minutes) the sections were mounted onto microscope slides with 0.5% gelatin solution and coverslipped using anti-fade mountant containing DAPI (Fluoroshield ™, Sigma-Aldrich, Clayton, Australia).

GFP, NOS1 and TH triple fluorescence immunohistochemistry

In order to determine whether OX_1-GFP expressing neurons also express NOS1 and/or TH, we performed triple-labelling fluorescence immunohistochemistry. The NOS1 and TH staining was carried out using a mouse anti-NOS1 antibody (Santa Cruz Biotechnology, CA; catalogue number: sc-5302, lot number: E2610) and a rabbit anti-TH antibody (Merck Millipore, Kilsyth, Australia; catalogue number: AB152, Lot number: 2219275), both extensively characterised in the past (Wang et al., 2011; Szot et al., 2012). To confirm the presence of OX1-GFP expression in neurons we used a mouse anti-nuclear antigen N (NeuN; 1:1000 dilution; Merck Millipore, Kilsyth, Australia, catalogue number: MAB377). A rabbit anti-glial fibrilliary acidic protein (GFAP; 1:2000 dilution; Dako, Sydney, Australia, catalogue number: Z0334) was also used to determine whether OX1-GFP was expressed in glia.

After sectioning, brainstem slices were rinsed with PBS containing Triton X-100 (0.3%) for 10 minutes. Sections were then incubated with the primary antisera (Chicken anti-GFP; 1:10,000 dilution; mouse anti-nNOS; 1:1000 dilution; and rabbit anti-TH; 1:2000 dilution) in PBS containing Triton X-100 (0.3%) for 1 hour at room temperature and then 24 hours at 4°C. Following repeated rinses in PBS (3 x 10 min) the sections were incubated for 1 hour at room temperature in PBS containing goat anti-Chicken Alexafluor 488 (1:500; Life Technologies, Australia) for visualisation of GFP, goat anti-mouse AlexaFluor 594 (1:500; Life Technologies, USA) for visualisation of NOS1 and goat anti-rabbit Alexafluor 680 (1:500; Jackson Immunoresearch Laboratories, PA, USA) for the visualisation of TH. Following further rinses in PBS (3 x 5 min), sections were mounted onto glass microscope slides in 0.5% gelatin and allowed to air dry for 10-15 minutes before being coverslipped with Fluoroshield™ (Sigma-Aldrich). In order to control for non-specific staining, sections were also processed in the absence of either the primary or secondary antisera.

Histological Analysis

A quantitative analysis of the labelling observed was made by counting the number of immunopositive neurons located within the defined borders of individual brainstem nuclei, as defined and delineated by the mouse brain atlas of Paxinos and Franklin (2001). All the stereotaxic co-ordinates and nomenclature were also adapted from the above atlas. The scoring system relied on the number of neurons judged by two independent investigators. The number of neurons counted was scored as: (-) <5 cells, (+) 6-10 cells, (++) 10-50 cells, (+++) >50 cells, (++++) >100 cells per brain nuclei per section.

Photomicroscopy and preparation of figures

The processed sections were examined on a confocal laser scanning microscope (Leica TCS SP8™; Leica GmbH, Wetzlar, Germany). Photomicrographs were taken with a Leica HyD™ detection and capture system using Leica Application Suite Advanced Fluorescence (LAS AF) software (LAS AF version 3.0, Leica GmbH, Wetzlar, Germany), saved as Leica Image files (.lif) and converted to TIFF images at 300 dpi resolution, and arranged in their respective sequences in Adobe Illustrator CS6 (version 16.0, Adobe, USA) for figure production.

Results

Validation of staining specificity

Incubation of mouse brainstem sections in the GFP antisera revealed robust staining that co-localised in exactly the same cells as those expressing intrinsic GFP fluorescence. No staining was observed in control brainstem sections from wildtype mice that do not express GFP. Incubation of mouse brain stem sections with the NOS1- and TH-antisera revealed the same patterns of distribution for nNOS (Gotti et al., 2005) and TH (Marcel et al., 1996; Puskás et al., 2010) staining previously reported in the mouse pons and brainstem. Omission of either the primary or secondary antisera resulted in the absence of staining.

Distribution of OX_1-GFP in the mouse brain stem

Staining for OX_1-GFP was observed in a number of discrete areas in the medulla oblongata and pons (Table 1). Both neuronal cell bodies and their proximal dendritic processes and axonal fibres were clearly labelled. The distribution of OX_1-GFP was consistent across all animals used in this study. A comparison of the quantity and location of OX_1-GFP labelling seen in the present study with the distribution of OX_1 mRNA reported by Marcus and colleagues (2001) are summarised in Table 2. In our study the staining was exclusively neuronal as revealed by double staining with the neuronal marker, NeuN (Figure 1A). We did not see any co-localisation when we double stained for the glia marker, glial fibrillary acidic protein (Figure 1B).

In the caudal medulla oblongata, very few cells were observed in the NTS (caudal of the area postrema) around the A2 noradrenergic region. Most of the cells were observed in the gracile nucleus (Figure 2A). Very limited OX_1-GFP positive cells were seen in the subpostremal NTS (one to two cells per 30 μm section). The only other group of OX_1-GFP positive cells was seen in the dorsal motor nucleus of the vagus nerve situated around the medial tip of the rostral NTS (Figure 2B,C). Many more cells were observed in the cuneate nuclei, and these cell groups extended throughout most of the rostro-caudal aspect of these nuclei.

In the ventral medulla, dense compact clusters of OX_1-GFP positive cells were observed in the lateral paragigantocellularis nucleus and ventral gigantocellular reticular cell group (Figure 3A). Tight clusters of cells were also seen in the raphe obscurus (Figure 3A), raphe pallidus (Figure 3A, 4D) nucleus, and more rostrally, the raphe magnus nucleus. No OX_1-GFP positive cells were observed in the RVLM, the compact formation of the nucleus ambiguus or the rostral ventromedial medulla (Figure 3A).

More rostral, towards the pons, cells were located close to the ventricular border of the magnocellular portion of the medial vestibular nucleus (at around bregma -6.0 mm). A small cluster of OX_1-GFP positive cells was seen in A5 region lateral to the facial nucleus. A tight cluster of large neurons were located in the inferior salivatory nucleus and a dense plexus of fibres was seen projecting ventrally from the salivatory nucleus towards the A5 area. In the raphe region, we observed substantial staining in the pontine raphe (Figure 4B) and median raphe nuclei (Figure 4C). We also observed a dense and compact cluster of OX_1-GFP positive cells in the A6 (or LC) region, but no expression was observed in either Barrington's nucleus (pontine micturition centre) or laterodorsal tegmental nucleus medial to the LC, or in the mesencephalic trigeminal nucleus bordering the LC laterally (Figure 5A). The positive cells extended ventrally towards the nucleus subcoeruleus where we also observed substantial staining. A small, elongated cluster of cells was also seen running along the medial borders of the medial longitudinal fasciculus near the midline.

Further rostral in the pons, towards the periaqueductal grey region, a dense collection of neurons was seen in the caudal and interfascicular subdivisions of the dorsal raphe nucleus (Figure 4A). A small cluster of cells was also distributed in the lateral dorsal tegmental area immediately ventral to the superior cerebral peduncle and the external cortex of the inferior colliculus (Figure 6A,B). OX1-GFP positive cells were also seen in the pedunculopontine tegmentum (Figure 6C), ventrolateral aspect of the dorsal raphe nucleus (Figure 6D) and

reticular tegmentum (Figure 6E). The ventral lateral periaqueductal grey contained a small number, less than 15 cells per section, of OX_1-GFP positive cells.

OX_1-GFP and NOS1 co-localisation

In the median raphe nucleus, cell bodies immunoreactive for OX_1-GFP and NOS1 were found to lie in close apposition, but no double-labelled cells were observed. OX_1-GFP and NOS1 co-localisation was seen predominantly in three areas of the brainstem and pons. In the medulla, co-localisation (OX_1-GFP neurons that were also NOS1-positive) was seen in the dorsal motor nucleus of the vagus nerve (64±9%), (Figure 2C), while in the pons, double staining was observed in both the A5 region (24±6%) and the pedunculopontine tegmentum (83±6%; Figure 6C). These data are summarised in Figure 7A.

OX1-GFP and TH co-localisation

OX_1-GFP and TH co-localisation was seen in a number of brain areas, and these are summarised in Figure 7B. The highest percentage of co-localisation (OX1-GFP neurons that were also TH-positive) was observed in the LC (94±4%; Figure 5D), followed by the lateral paragigantocelluris cell group (85±4%; Figure 3D) situated in the ventral medulla, immediately dorsal and lateral of the inferior olives. OX_1-GFP and TH double-labelling was also seen in the median raphe (Figure 5C), raphe magnus, raphe obscurus and raphe pallidus nuclei (Figure 5D). A smaller percentage (15±3%) of OX_1-GFP cells located in the A5 region were also TH immunoreactive.

Discussion

In the present study we systematically mapped the anatomical distribution of OX_1-GFP expression throughout the brain stem and pons of OX_1-GFP transgenic reporter mice. We observed discrete and specific expression in a number of nuclei distributed throughout the medulla oblongata and pons. Although our results are highly consistent with the distribution of OX_1 mRNA, we failed to detect OX_1 receptor expression in areas of the medulla where OX_1 receptor protein expression has previously been described (Hervieu et al., 2001; Shahid et al., 2012). This calls into question the specificity of some antibodies previously used. Co-labelling of OX_1-GFP expression with NOS1 and TH revealed co-localisation of NOS1 and OX_1-GFP in only a few discrete nuclei (*viz*, dorsal vagal motor nucleus, A5 region and pedunculopontine tegmentum). TH and OX_1-GFP co-localisation was mainly found in the LC, raphe nuclei and the lateral paragigantocellularis cell group, but not in the rostal ventrolateral or rostral ventromedial medulla. While we observed OX_1-GFP positive cells double labelled for either NOS1 or TH immunoreactivity, only very few triple-labelled cells were observed and represented a small percentage of OX_1-GFP cells quantified.

Caveats and limitations

The expression and localisation of certain G-protein coupled receptors has been difficult to study and systematically map largely due to a lack of specific antibodies. Using reporter genes to tag selected neuronal populations is an important approach, enabling investigators to overcome this limitation and perform anatomical and physiological studies that were previously difficult. However, the use of reporter genes is not without limitations. For example, substantial variability in the pattern of GFP expression among mice generated from the same construct has been previously reported (Feng et al., 2000). However, in the present study we observed very consistent expression of OX_1-GFP within the medulla oblongata and pons in all mice used. This is not unexpected as variations are minimal among descendants of a single founder (Feng et al., 2000). There has also been some evidence of over- or under-reporting of reporter genes (Sun et al., 2014). Here, we undertook a detailed

comparison of the expression patterns of OX_1-GFP with the OX_1 mRNA previously reported (Marcus et al., 2001) and see faithful recapitulation of the endogenous OX_1 gene expression pattern. Importantly, we did not see ectopic expression where none had been reported previously (Marcus et al, 2001), suggesting that it is unlikely that the transgenic reporter mouse line we used is over-reporting. Another potential limitation of the study relates to the labelling of fine dendritic processes that project some distance away from the cell body. While we observed dendritic labelling close to the neuronal cell bodies expressing OX_1-GFP, we did not find dendritic or nerve terminal labelling in areas where we did not see OX_1-GFP positive cell bodies.

There was generally excellent agreement between the expression of OX_1-GFP in the pons and medulla oblongata found in the present study with the mRNA expression described previously by Marcus and colleagues in rat brain (2001; see Table 2). They reported dense mRNA expression in structures such as the LC, A5 noradrenergic cell group, and the various raphe nuclei, areas where we recorded clear OX_1-GFP expression. Marcus et al (2001) reported no mRNA expression in areas such as Barrington's nucleus, hypoglossal nucleus and the nucleus ambiguus – areas where we also did not see OX_1-GFP expression in cells. The study of Hervieu et al., (2001) looked at the expression of OX_1 receptor mRNA and protein in pontine and brain stem areas in a more limited and less comprehensive manner. They reported OX_1 receptor immunoreactivity in the LC, spinal trigeminal nucleus, medial vestibular nucleus and gigantocellular reticular nucleus, which is in agreement with the distribution we see in the present study. However, they also reported dense immunohistochemical staining within the olivary complex and the facial nucleus, two areas where we did not see any OX_1-GFP positive cells or dendritic processes. We believe these discrepancies are primarily due to the challenging task of producing antibodies that are specific for G-protein coupled receptors.

When injected into the 4th ventricle, both low and high doses of orexin-A increase food intake over a 2-hour period, an effect that was blocked by the selective OX_1 receptor antagonist, SB334867 (Parise et al., 2011). These data suggest that orexin-A in the hindbrain plays a role in regulating food intake. However, we observed very few OX_1-GFP positive cells within the NTS and none within the area postrema. This was somewhat unexpected as Parise and colleagues (2011) describe fairly dense networks of Orexin-A positive fibres apposing putative amylin containing cells within the NTS and AP in rats. Moreover, we did not see any OX_1-GFP positive cells or dendritic processes in the regions of the AP where Parise and colleagues saw Fos labelling following 4th ventricular injections of orexin-A. This suggests that the orexin-A released in the AP is more likely to act on OX_2 and not OX_1 receptors. Microinjection of orexin-A into the NTS of urethane-anaesthetised rats elicits increases in both blood pressure and heart rate (Smith et al, 2002a). Given that orexin-B also elicits similar cardiovascular responses, the authors suggested that the OX_2 receptor might be responsible for the cardiovascular actions of both orexin-A and orexin-B within the caudal NTS (Smith et al., 2002a). This is supported by electrophysiological studies showing that orexin-B stimulates almost half (48%) of all NTS cells tested (Smith et al., 2002b). These, together with our findings, are consistent with the Allen Brain Atlas, which shows higher expression of the OX_2 than OX_1 mRNA within the AP and NTS of the mouse brain. We cannot, however, rule out the possibility that our staining method was not sensitive enough to label all dendritic and terminal processes expressing the OX_1 receptor. Hence, while there appears to be limited expression of OX_1 receptors in the caudal NTS, we cannot rule out the possibility of OX_1 receptor expression on dendrites and nerve terminals in this area. Moreover, we cannot discount the possibility that there might be species (and/or strain) differences in the expression of OX_1 receptors between rats and mice; however, our finding of similar expression patterns of OX_1-GFP in mice compared with OX_1 mRNA in rats (Marcus et al., 2001) suggests that may not be the case.

Microinjection of orexin-A into the RVLM of conscious rats elicits increases in both blood pressure and heart rate (Machado et al., 2002). More recent studies have demonstrated the presence of both OX_1 and OX_2 receptors within the rat RVLM and similarly that bilateral microinjections of orexin-A evokes pressor, tachycardic and sympathoexcitatory responses in a dose-dependent manner (Shahid et al., 2012; Xiao et al., 2013). These effects were attenuated with prior treatment with SB334867 (Shahid et al., 2012) and SB408124 (Xiao et al., 2004), selective OX_1 receptor antagonists, suggesting that the responses were predominantly mediated by OX_1 receptors. These investigators went on to show expression of both OX_1 and OX_2 receptors on both TH and non-TH positive C1 cells (Shahid et al., 2012) and neuronal nitric oxide synthase and inducible nitric oxide synthase expressing cells (Xiao et al., 2013) within the RVLM by immunohistochemistry. In the present study, we did not see any OX_1-GFP labelling within the RVLM in our GFP transgenic reporter mice. Much of the expression was located in the lateral paragigantocellularis cell group located just medial of the RVLM towards the inferior olives. We therefore propose that, either the effects of orexin-A are predominantly mediated by the OX_2 receptor within the rat RVLM (as the OX_1 selective antagonist only partially attenuated the response), or that there might be a species difference in the expression of OX_1 receptors within the RVLM of rats and mice.

In the past, there has been little distinction between the lateral paragigantocellularis nucleus and the RVLM. Therefore, it is conceivable that the microinjection might have spread to the lateral paragigantocelluar nucleus, which we have shown to contain OX_1-GFP expressing neurons. There is now good evidence that the RVLM and lateral paragiantocellular nucleus are distinct cell groups (Paxinos & Franklin, 2001) and both play a role in controlling sympathetic function (Carrive & Gorissen, 2008). Additionally, while we observed robust cell body and dendritic staining that was in close proximity to the OX_1-GFP neuron cell bodies, it is possible that our staining method lacked the sensitivity to label more distally located dendritic fibres and nerve terminals. As such, it is also conceivable that the responses described could result from the activation of OX_1 receptors located on distal dendritic

processes or terminal fields. Our findings are more consistent with the study of Huang and colleagues (2010). They reported that rat RVLM neurons predominantly express OX_2, as opposed to the OX_1 receptors, which might explain the effects of Orexin-A when exogenously applied to the RVLM. Our finding of OX_1 receptor expression in the lateral paragigantocellular cell group is also supported by functional studies reporting that orexin-A, via OX_1 receptors have an antinociceptive action to thermal (hot plate) and chemical (formalin) stimulation when microinjected into the lateral paragigantocellular nucleus of conscious rats – a response that was blocked by the selective OX_1 receptor antagonist, SB334867 (Erami et al., 2012).

The LC is known to receive the most dense orexinergic innervation within the mammalian central nervous system (Hagan et al., 1999; Horvath et al., 1999; Puskás et al., 2010). We observed high levels of OX_1-GFP expression within the LC and the majority (>94%) of the cells were co-localised with TH. This was not an unexpected finding as high OX_1 mRNA expression has been previously reported in this nucleus (Marcus et al., 2001; Hervieu et al., 2001). The effects of orexin-A within the LC have been well documented. Exogenous application of orexin-A increases the firing rate of LC neurons and when administered at the onset of the normal sleep period, induced a significant increase in arousal during the second and third hour after administration (Hagan et al., 1999). Orexin-A also caused a significant increase in locomotor activity. Interestingly, knocking down the OX_1 receptor with short interfering RNAs in the LC increased rapid eye movement sleep (Chen et al., 2010).

While the LC showed the greatest expression of OX_1-GFP, strong expression was also observed in the dorsal raphe nucleus (DRN). The DRN has been shown to play a role in modulation of the sleep wake cycle and in processing the sensation of pain (Wang et al., 1994). When orexin-A was directly applied to the DRN via reverse microdialysis, it caused the release of 5-HT in a dose-dependent manner (Tao et al., 2006). Hence, orexin-A appears to excite the OX_1 receptor subtype within the DRN to increase 5-HT release to mediate

wakefulness. Application of orexin-B was far less effective within the DRN, suggesting that the OX_1 receptor subtype is the predominant receptor expressed within this nucleus. These functional, *in vivo,* findings are consistent with our present histological findings.

Conclusion

Using an OX_1-GFP transgenic reporter mouse, we extensively mapped the anatomical distribution of OX_1 receptors and their co-localisation with NOS1 and TH throughout the medulla oblongata and pons. Our results are in agreement with the reported expression of OX_1 receptor mRNA in the rat brainstem and pons (Marcus et al., 2001). However, to the best of our knowledge, no other study has systematically mapped the OX_1 receptor protein in the mouse brain. Based on the distribution of OX_1-GFP, our results support the involvement of orexin-A in the regulation of a number of physiological and behaviour functions, such as the regulation of arousal, the sleep-wake cycle, control of feeding and in mood regulation. The absence or limited expression of OX_1-GFP in the RVLM and NTS suggests that the OX_2 receptor might be the principle effector of either the orexin-A or orexin-B peptides within these structures.

Acknowledgements:

We thank Dr Danny Winder (Vanderbilt) and Dr Paul Kenny (Mount Sinai School of Medicine) for the OX_1R-eGFP founder mice. This work was supported by the National Health and Medical Research Council (NH&MRC; Australia) and the Victorian Government through the Operational Infrastructure Scheme. LCB is supported by a NH&MRC Early Career Fellowship. CNM and AJL are supported by NH&MRC Research Fellowships (566819 and 1020737 respectively).

References

Antunes VR, Brailoiu GC, Kwok EH, Scruggs P, Dun NJ (2001) Orexins/hypocretins excite rat sympathetic preganglionic neurons in vivo and in vitro. Am J Physiol, 281: R1801-R1807.

Carrive P (2013) Orexin, orexin receptor antagonists and central cardiovascular control. Front Neurosci, 7: 257 [doi: 10.3389/fnins.2013.00257]

Carrive P, Gorissen M (2008) Premotor sympathetic neurons of conditioned fear in the rat. Eur J Neurosci, 28: 428-446.

Chen L, McKenna JT, Bolortuya Y, Winston S, Thakkar MM, Basheer R, Brown RE, McCarley RW. (2010) Knockdown of orexin type 1 receptor in rat locus coeruleus increases REM sleep during the dark period. Eur J Neurosci. 32: 1528-1536.

Ciriello J, Caverson MM, McMurray JC, Bruckschwaiger EB (2013) Co-localization of hypocretin-1 and leucine-enkephalin in hypothalamic neurons projecting to the nucleus of the solitary tract and their effect on arterial pressure. Neuroscience, 250: 599-613.

Date Y, Ueta Y, Yamashit H, Yamguchi H, Matsukura S, Kangawa K, Sakurai T, Yanagisawa M, Nakazato M (1999) Orexins, orexigenic hypothalamic peptides, interact with autonomic neuroendocrine and neuroregulatory systems. Proc Natl Acad Sci, 96: 748-753.

Erami E, Azhdari-Zarmehri H, Ghasemi-Dashkhasan E, Esmaeili MH, Semnanian S (2012) Intra-paragigantocellularis lateralis injection of orexin-A has an antinociceptive effect on hot plate and formalin tests in rat. Brain Res, 1478: 16-23.

Feng G, Mellor RH, Bernstein M, Keller-Peck C, Nguyen QT, Wallace M, Nerbonne JM, Lichtman JW, Sanes JR (2000) Imaging neuronal subsets in transgenic mice expressing multiple spectral variants of GFP. Neuron, 28: 41–51.

Ginovart N, Marcel D, Bezin L, Garcia C, Gagne C, Pujol JF, Weissmann D. (1996) Tyrosine hydroxylase expression within Balb/C and C57black/6 mouse locus coeruleus. I. Topological organization and phenotypic plasticity of the enzyme-containing cell population. Brain Res, 721: 11-21.

Gotti S, Sica M, Viglietti-Panzica C, Panzica G. (2005) Distribution of nitric oxide synthase immunoreactivity in the mouse brain. Microsc Res Tech, 68: 13-35.

Hagan JJ, Leslie RA, Patel S, Evans ML, Wattam TA, Holmes S, Benham CD, Taylor SG, Routledge C, Hemmati P, Munton RP, Ashmeade TE, Shah AS, Hatcher JP, Hatcher PD, Jones DN, Smith MI, Piper DC, Hunter AJ, Porter RA, Upton N (1999) Orexin A activates locus coeruleus cell firing and increases arousal in the rat. Proc Natl Acad Sci USA, 96: 10911-10916.

Hervieu GJ, Cluderay JE, Harrison DC, Roberts JC, Leslie RA (2001) Gene expression and protein distribution of the orexin-1 receptor in the rat brain and spinal cord. Neuroscience. 103: 777-997.

Ho YC, Lee HJ, Tung LW, Liao YY, Fu SY, Teng SF, Liao HT, Mackie K, Chiou LC (2011) Activation of orexin 1 receptors in the periaqueductal gray of male rats leads to antinociception via retrograde endocannabinoid (2-arachidonoylglycerol)-induced disinhibition. J Neurosci, 31: 14600-14610.

Horvath TL, Peyron C, Diano S, Ivanov A, Aston-Jones G, Kilduff TS, van Den Pol AN (1999) Hypocretin (orexin) activation and synaptic innervation of the locus coeruleus noradrenergic system. J Comp Neurol, 415: 145-159.

Huang SC, Dai YW, Lee YH, Chiou LC, Hwang LL. (2010) Orexins depolarize rostral ventrolateral medulla neurons and increase arterial pressure and heart rate in rats mainly via orexin 2 receptors. J Pharmacol Exp Ther. 334: 522-529.

Inutsuka A, Yamanaka A (2013) The physiological role of orexin/hypocretin neurons in the regulation of sleep/wakefulness and neuroendocrine functions. Front Endocrinol, 4: 18 [doi: 10.3389/fendo.2013.00018].

Kay K, Parise EM, Lilly N, Williams DL (2014) Hindbrain orexin 1 receptors influence palatable food intake, operant responding for food, and food-conditioned place preference in rats. Psychopharmacology, 231: 419-427.

Lawrence AJ (2010) Regulation of alcohol-seeking by orexin (hypocretin) neurons. Brain Res, 1314: 124-129.

Leinders-Zufall T, Ishii T, Chamero P, Hendrix P, Oboti L, Schmid A, Kircher S, Pyrski M, Akiyoshi S, Khan M, Vaes E, Zufall F, Mombaerts P (2014) A family of nonclassical class I MHC genes contributes to ultrasensitive chemodetection by mouse vomeronasal sensory neurons. J Neurosci, 34: 5121-5133.

Llewellyn-Smith IJ, Reimann F, Gribble FM, Trapp S (2011) Preproglucagon neurons project widely to autonomic control areas in the mouse brain. Neuroscience, 180: 111-121.

Machado BH, Bonagamba LG, Dun SL, Kwok EH, Dun NJ (2002) Pressor responses to microinjection of orexin/hypocretin into rostral ventrolateral medulla of awake rats. Reg Pept, 104: 75-81.

Marcus JN, Aschkenasi CJ, Lee CE, Chemelli RM, Saper CB, Yanagisawa M, Elmquist JK. (2001) Differential expression of orexin receptors 1 and 2 in the rat brain. J Comp Neurol, 435: 6-25.

Parise EM, Lilly N, Kay K, Dossat AM, Seth R, Overton JM, Williams DL (2001) Evidence for the role of hindbrain orexin-1 receptors in the control of meal size. Am J Physiol Regul Integr Comp Physiol, 301: R1692-R1699.

Paxinos G, Franklin KBJ (2001) The mouse brain in stereotaxic coordinates. Academic Press, San Diego, USA.

Puskás N, Papp RS, Gallatz K, Palkovits M (2010) Interactions between orexin-immunoreactive fibers and adrenaline or noradrenaline-expressing neurons of the lower brainstem in rats and mice. Peptides, 31: 1589-1597.

Sakurai T, Amemiya A, Ishii M, Matsuzaki I, Chemelli RM, Tanaka H, Williams SC, Richardson JA, Kozlowski GP, Wilson S, Arch JR, Buckingham RE, Haynes AC, Carr SA, Annan RS, McNulty DE, Liu WS, Terrett JA, Elshourbagy NA, Bergsma DJ, Yanagisawa M. (1998) Orexins and orexin receptors: a family of hypothalamic neuropeptides and G protein-coupled receptors that regulate feeding behavior. Cell, 94: 573-585.

Shih CD1, Chuang YC (2007) Nitric oxide and GABA mediate bi-directional cardiovascular effects of orexin in the nucleus tractus solitarii of rats. Neuroscience, 149: 625-635.

Shahid IZ, Rahman AA, Pilowsky PM, (2012) Orexin A in rat rostral ventrolateral medulla is pressor, sympatho-excitatory, increases barosensitivity and attenuates the somato-sympathetic reflex. Br J Pharmacol. 165: 2292-2303.

Smith PM, Connolly BC, Ferguson AV (2002a) Microinjection of orexin into the rat nucleus tractus solitarius causes increases in blood pressure. Brain Res, 950: 261-267.

Smith BN, Davis SF, Van Den Pol AN, Xu W (2002b) Selective enhancement of excitatory synaptic activity in the rat nucleus tractus solitarius by hypocretin 2. Neuroscience, 115: 707-714.

Soya S, Shoji H, Hasegawa E, Hondo M, Miyakawa T, Yanagisawa M, Mieda M, Sakurai T (2013) Orexin receptor-1 in the locus coeruleus plays an important role in cue-dependent fear memory consolidation. J Neurosci, 33:14549-14557.

Sun M-Y, Yetman MJ, Lee T-C, Chen Y, Jankowsky JL (2014) Specificity and efficiency of reporter expression in adult neural progenitors vary substantially among nesting-CreERT2 lines. J Comp Neurol, 522: 1191-1208.

Szot P, Knight L, Franklin A, Sikkema C, Foster S, Wilkinson CW, White SS, Raskind MA (2012) Lesioning noradrenergic neurons of the locus coeruleus in C57Bl/6 mice with unilateral 6-hydroxydopamine injection, to assess molecular, electrophysiological and biochemical changes in noradrenergic signaling. Neuroscience, 216: 143-157.

Tao R, Ma Z, McKenna JT, Thakkar MM, Winston S, Strecker RE, McCarley RW (2006) Differential effect of orexins (hypocretins) on serotonin release in the dorsal and median raphe nuclei of freely behaving rats. Neuroscience. 141: 1101-1105.

Tupone D, Madden CJ, Cano G, Morrison SF (2011) An orexigenic projection from the perifornical hypothalamus to raphe pallidus increases rat brown adipose tissue thermogenesis. J Neurosci, 31: 15944-15955.

Wang LL, Zhao XC, Yan LF, Wang YQ, Cheng X, Fu R, Zhou LH (2011) C-jun phosphorylation contributes to down regulation of neuronal nitric oxide synthase protein and motoneurons death in injured spinal cords following root-avulsion of the brachial plexus. Neuroscience. 189: 397-407.

Wang Q-P, Nakai Y (1994) Dorsal raphe: an important nucleus in pain modulation. Brain Res Bull, 34: 575-585

Xiao F, Jiang M, Du D, Xia C, Wang J, Cao Y, Shen L, Zhu D. (2013) Orexin A regulates cardiovascular responses in stress-induced hypertensive rats. Neuropharmacology, 67:16-24.

Xu TR, Yang Y, Ward R, Gao L, Liu Y (2013) Orexin receptors: multi-functional therapeutic targets for sleeping disorders, eating disorders, drug addiction, cancers and other physiological disorders. Cell Signal, 25: 2413-2423.

Yao ST, Gouraud SS, Qiu J, Cunningham JT, Paton JF, Murphy D (2012) Selective up-regulation of JunD transcript and protein expression in vasopressinergic supraoptic nucleus neurones in water-deprived rats. J Neuroendocrinol, 24: 1542-1552.

Table 1: Distribution OX_1-GFP in the mouse brainstem and pons

dist from Bregma (mm)	Abbr	Brain Nucleus	
-7.92	Cu	Cuneate nucleus	+
	NTS	Nucleus of the solitary tract	+
	Rob	Raphe obscurus	+
-7.76	10N	Dorsal motor nucleus of the vagus	-
	12N	hypoglossal nucleus	-
	Cu	Cuneate nucleus	-
	Gr	Gracile nucleus	++
	NTS	Nucleus of the solitary tract	+
	PMn	Paramedian reticular nucleus	-
	Sp5C	Spinal trigeminal nucleus, caudal	++
-7.56	Cu	Cuneate nucleus	+
	10N	Dorsal motor nucleus of the vagus	+
	NTS	Nucleus of the solitary tract	-
-7.08	10N	Dorsal motor nucleus of the vagus	+
	LPGi	Lateral paragigantocellular nucleus	+
	ROb	Raphe obscurus	++
-6.84	Amb	Nucleus ambiguus	-
	LPGi	Lateral paragiantocellular	++
	Mve	Medial vestibular nucleus	+
	ROb	Raphe obscurus	++
	RPa	Raphe pallidus	++
-6.72	Amb	Nucleus ambiguus	-
	GiV	Gigantocellular reticular nucleus	++
	ROb	Raphe obscurus	++
	RPa	Raphe pallidus	++
	RVL	Rostral ventrolateral medulla	-
-6.48	10N	Dorsal motor nuclues vagus	+
	MVePC	Medial vestibular nucleus, parvicellular part	+
	RMg	Raphe magus	++
	RPa	Raphe pallidus	++
-6.24	RPa	Raphe pallidus	++
	SolIM	Nucleus of solitary tract, intermediate part	+
-6	MVeMC	Medial vestibular nucleus, magnocellular part	+

	PCRtA	Parvicellular reticular nucleus	+
	RPa	Raphe pallidus	++
-5.8	A5	A5 noradrenergic cell group	++
	IS	Inferior salivatory nucleus	+
	MVePC	Medial vestibular nucleus, parvicellular part	+
	RMg	Raphe magus	+
	RPa	Raphe pallidus	++
-5.5	LC	Locus coeruleus	++++
	RMg	Raphe magus	++
	RPa	Raphe pallidus	+
-5.34	DRI	Dorsal raphe nucleus, infascicular part	+
	LC	Locus coeruleus	++++
	PnR	Pontine raphe nucleus	++
	RMg	Raphe magus	++
	SubCD	Nucleus sub-coeruleus	++
-5.02	ECIC (2)	External cortex of the inferior colliculus	++
	LDTg	Laterodorsal tegmental nucleus	++
	LPAG	Lateral periaqueductal grey	+
	MnR	Median raphe nucleus	++
	PPTg	Pedunculopontine tegmental nucleus	++
-4.84	DRVL	Dorsal raphe nucleus, ventrolateral part	+++
	PPTg	Pedunculopontine tegmental nucleus	++
	RtTg	Reticulotegmental nucleus of the pons	++
-4.6	BIC	Nucleus of the brachium of the inferior colliculus	+
	DLPAG	Dorsolateral periaqueductal grey	+
	DMPAG	Dorsomedial periaqueductal grey	+
	DRD	Dorsal raphe nucleus, dorsal part	++
	DRVL	Dorsal raphe nucleus, ventrolateral part	+++
	Mo5	Motor trigeminal nucleus	+
	RtTg	Reticulotegmental nucleus of the pons	++

-	< 5 cells / section
+	6-10 cells/section
++	10-50 cells/section
+++	>50 cells/section
++++	>100 cells/section

TABLE 2 Comparision of OX_1-GFP distribution (this paper) with OX_1 receptor mRNA distribution (Marcus et al, 2001).

	OX_1-GFP	OX_1 mRNA
A5 noradrenergic cell group	++	+++
Barrington's nucleus	-	-
Cuneate nucleus	+	nd
Dorsal motor nucleus of the vagus	+	++
Dorsal raphe nucleus, ventrolateral part	+++	++
Dorsolateral periaqueductal gray	+	++
Dorsomedial periaqueductal gray	+	++
External cortex of the inferior colliculus	++	+
Gracile nucleus	++	nd
Hypoglossal nucleus	-	-
Inferior salivatory nucleus	+	nd
Lateral paragigantocellular nucleus	+	nd
Laterodorsal tegmental nucleus	++	++
Locus coeruleus	++++	+++
Medial vestibular nucleus	+	+
Nucleus ambiguus	-	-
Nucleus of the solitary tract	+	++
Nucleus sub-coeruleus	++	nd
Nuclues of the brachium of the inferior colliculus	+	-
Paramedian reticular nucleus	-	nd
Parvicellular reticular nucleus	+	nd
Pedunculopontine tegmental nucleus	++	++
Pontine raphe Nucleus	++	nd
Raphe magus nucleus	++	+
Raphe obscurus nucleus	++	++
Reticulotegmental nucleus of the pons	++	++
Spinal trigeminal nucleus	++	-

Figure Legends

Figure 1. Representative confocal photomicrographs of double-immunofluorescence for green fluorescent protein (GFP; green), and A) the neuronal marker, NeuN, B) the glia marker glial fibrilliary acid protein, GFAP in the pedunculopontine tegmental nucleus of the pons. OX1-GFP double-staining was co-localised with NeuN (indicated by the white arrow-heads) but not GFAP. Scale bar: 50µm.

Figure 2. Representative confocal photomicrographs of triple-immunoflourescence for green fluorescent protein (GFP; green), tyrosine hydroxylase (TH; purple) and neuronal nitric oxide synthase (NOS1; red) in the dorsal medulla of the OX_1-GFP reporter mouse. OX_1-GFP expression was seen in the gracile nucleus (A) and the dorsal motor nucleus of the vagus (B). Photomicrographs taken at higher magnification (of the area represented by the box bordered by dotted lines in (B) demonstrate double staining for GFP and NOS1, but not TH (C). Abbreviations: AP, area postrema; CC, central canal; Gr, gracile nucleus; NTS, nucleus of the solitary tract. Arrowheads indicate cells that are OX_1-GFP and NOS1 positive. Scale bars: 200µm in A,B; 100µm in C.

Figure 3. Representative confocal photomicrographs of triple-immunoflourescence for green fluorescent protein (GFP; green), tyrosine hydroxylase (TH; purple) and neuronal nitric oxide synthase (NOS1; red) in the ventral medulla of the OX_1-GFP reporter mouse. OX_1-GFP expression was seen in the raphe pallidus, raphe obscurus and the ventral gigantocellular reticular cell group (A). Immunostaining for TH (B) and NOS1 (C) revealed co-localisation of OX_1-GFP with TH (indicated by the white arrow-heads), but not NOS1 (D). The inserts shown in each panel shows the region delineated by the dashed rectangles at higher magnification. Abbreviations: Amb, nucleus ambiguus; GiV, ventral gigantocellular reticular cell group; py, pyramidal tract; ROb, raphe obscurus; RPa, raphe pallidus; RVL, rostral

ventrolateral medulla; sp5, spinal trigeminal tract. Scale bar: 200µm in A, B, C, D; 50µm in A', A'', B', B'', C', C'', D', D'').

Figure 4. Representative confocal photomicrographs of triple-immunoflourescence for green fluorescent protein (GFP; green), tyrosine hydroxylase (TH; purple) and neuronal nitric oxide synthase (NOS1; red) in the raphe regions. OX_1-GFP expression was seen in the dorsal raphe (A), pontine raphe (B) and median raphe (C) nuclei, and the raphe pallidus (D). Triple immunostaining revealed co-localisation of OX_1-GFP with TH, but not NOS1. Abbreviations: Aq, aqueduct; DR, dorsal raphe; mlf, medial longitudinal fasciculus. Arrowheads point to cells that are OX_1-GFP and TH positive. Scale bars: 200µm in A,C; 50µm in B; 100µm in D.

Figure 5. Confocal photomicrographs of triple-immunoflourescence for green fluorescent protein (GFP; green), tyrosine hydroxylase (TH; purple) and neuronal nitric oxide synthase (NOS1; red) in the region of the locus coeruleus (LC). OX_1-GFP expression was predominantly seen in the LC, but not medially in Barrington's nucleus or laterally in the mesencephalic trigeminal nucleus. Triple immunostaining with TH (B) and NOS1 (C) revealed extensive co-localisation of OX_1-GFP with TH, but not NOS1 (D). Abbreviations: Bar, Barrington's nucleus; Cb, cerebellum; DTgC dorsal tegmentum, central part; LC, locus coeruleus; LDTg, laterodorsal tegmentum; LPB, lateral parabrachial nucleus; Me5, mesencephalic trigeminal nucleus; MPB, medial parabrachial nucleus; mlf, medial longitudinal fasciculus; scp, superior cerebral peduncle. Scale bar: 500µm

Figure 6. Confocal photomicrographs of double-immunoflourescence for green fluorescent protein (GFP; green) and neuronal nitric oxide synthase (NOS1; red) in the rostral pons around the periaqueductal grey (A). OX_1-GFP positive cells were seen in the external cortex of the inferior colliculus (B), pedunculopontine tegmental nucleus (C), ventolateral portion of the dorsal raphe nucleus (D) and the reticulotegmental nucleus of the pons (E). Double staining for OX_1-GFP and NOS1 was only seen in the pedunculopontine tegmental nucleus

at this level of the pons, as indicated by the white arrowheads. Abbreviations: Aq, aqueduct; ECIC, external cortex of the inferior colliculus; DRVL, ventolateral portion of the dorsal raphe; PPTG, pedunculopontine tegmental nucleus; RPO, rostral periolivary region; RtTg, reticulotegmental nucleus of the pons. Scale bars: 100μm in B,C,D,E.

Figure 7. These graphs show the extent of OX_1-GFP co-localisation with neuronal (A) nitric oxide synthase (NOS1) and (B) tyrosine hydroxylase (TH) in the brainstem and pons of the OX_1-GFP reporter mouse. Data are shown as the mean ± SE (n=5). Abbreviations: 10N, dorsal motor nucleus of the vagus; A5, A5 noradrenergic cell group; LC, locus coeruleus; LPGi, lateral paragigantocellularis; MnR, median raphe nucleus; PPTg, pedunculopontine tegmental nucleus; RMg, raphe magnus; ROb, raphe obscurus; RPa, raphe pallidus.

Figure 1

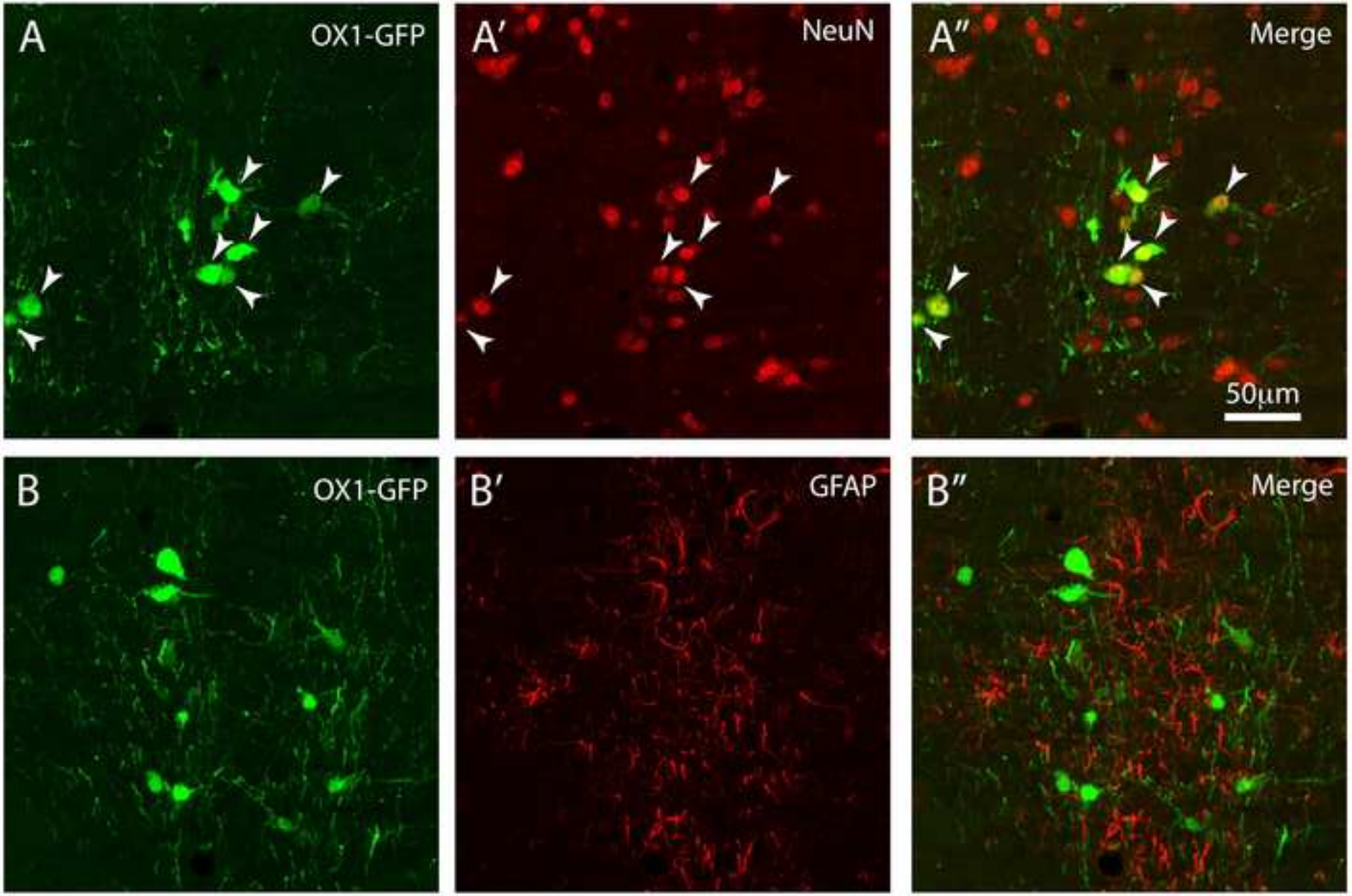

Figure 2

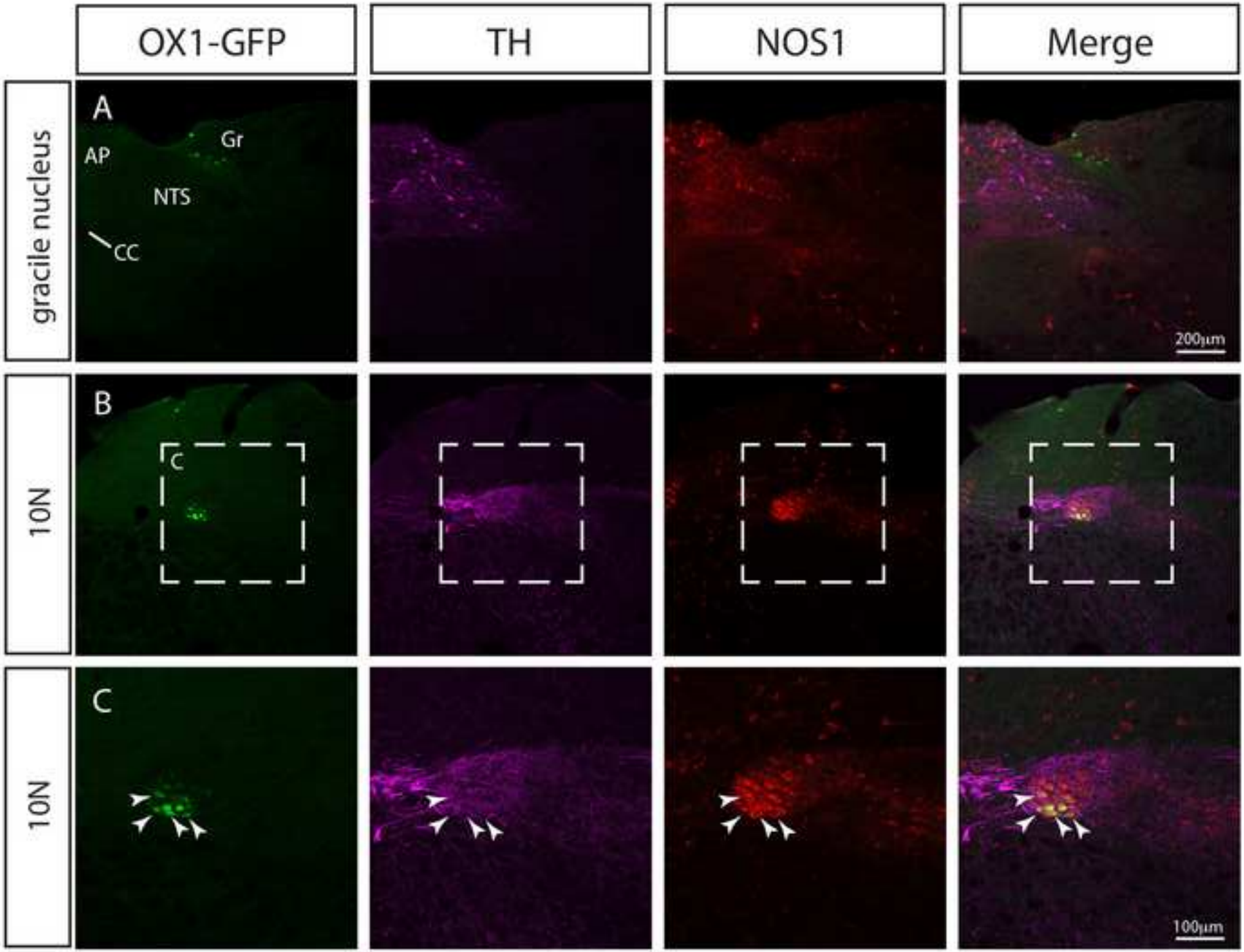

Figure 3 insets

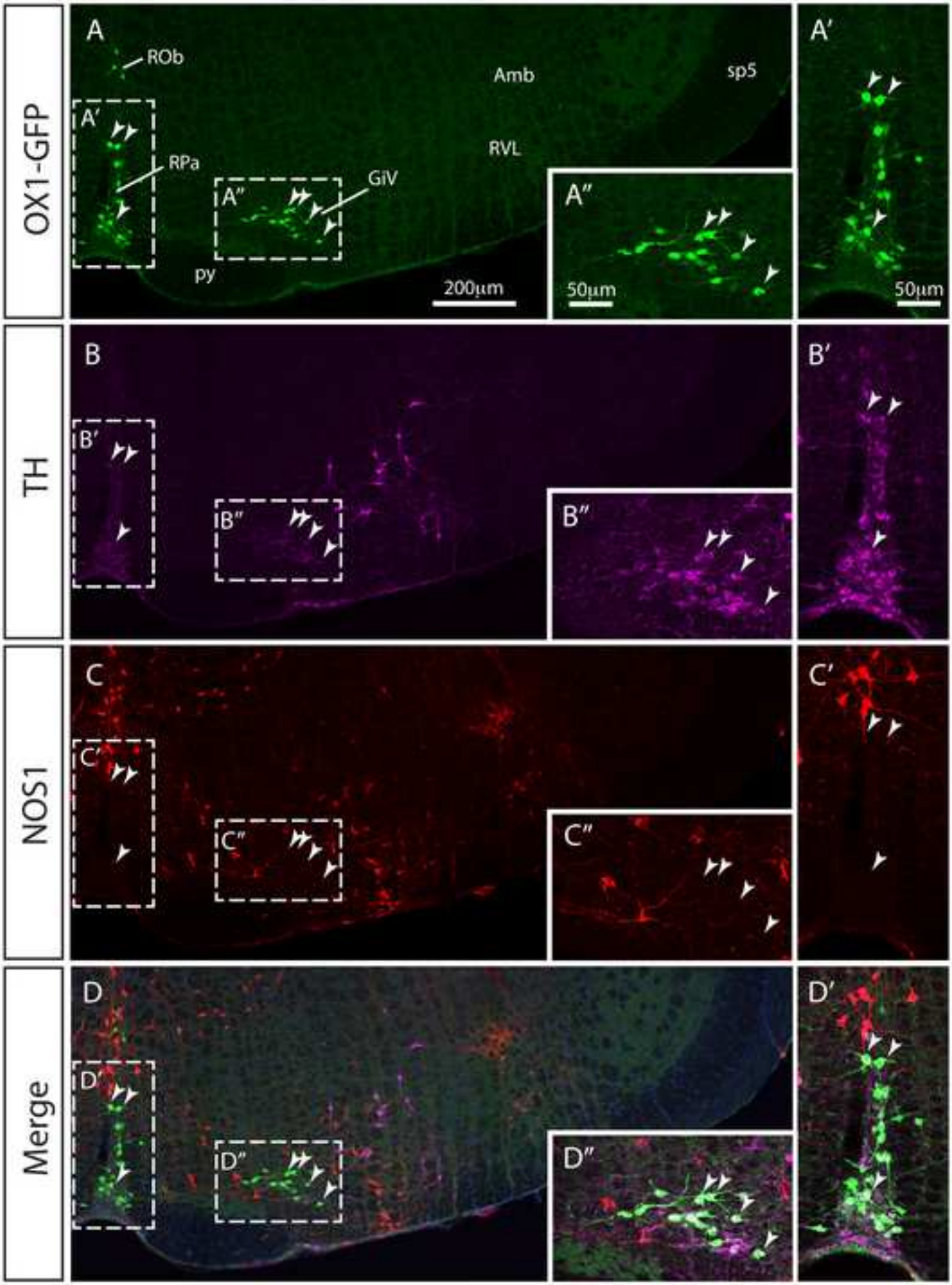

Figure 4

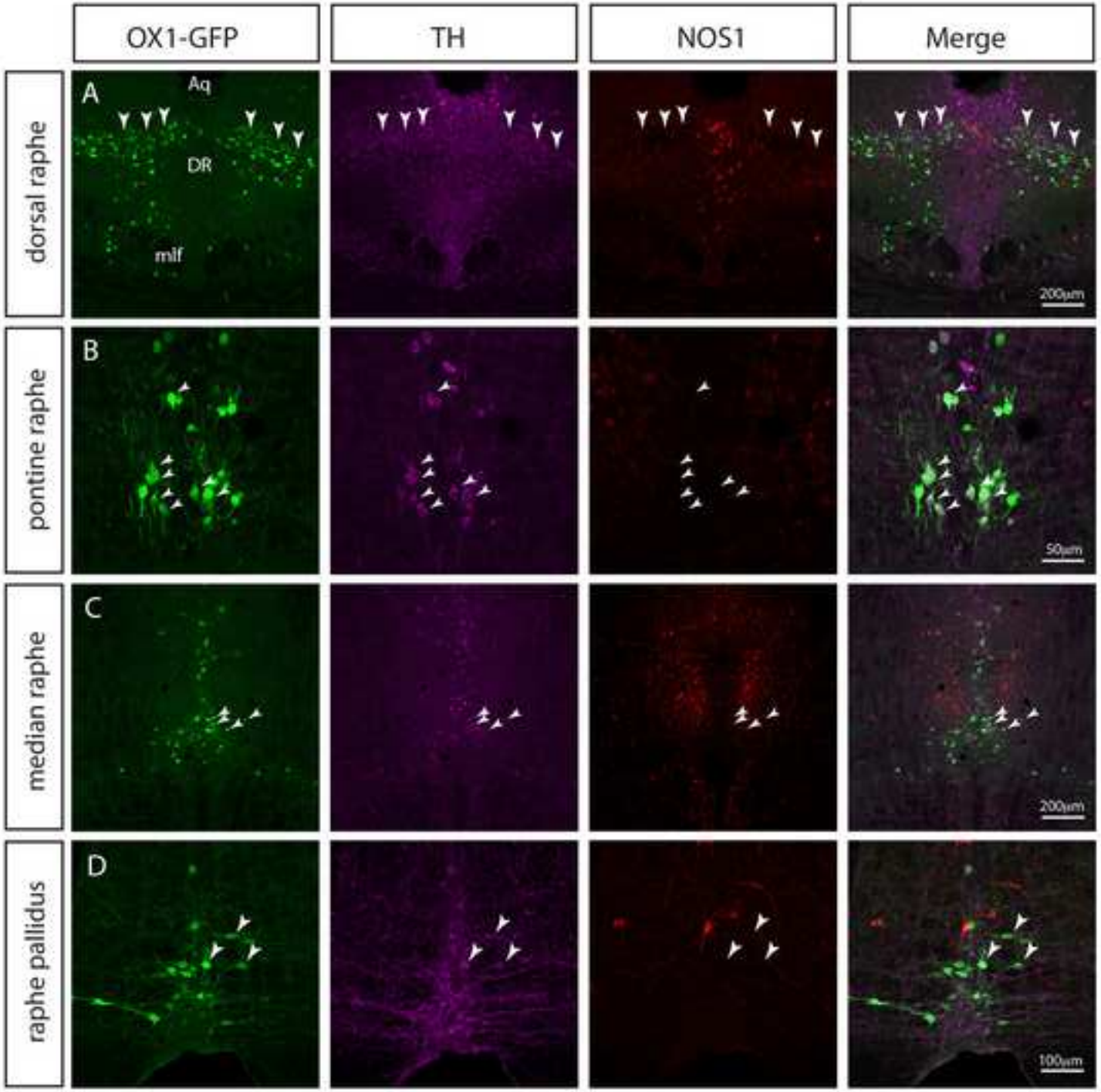

Figure 5

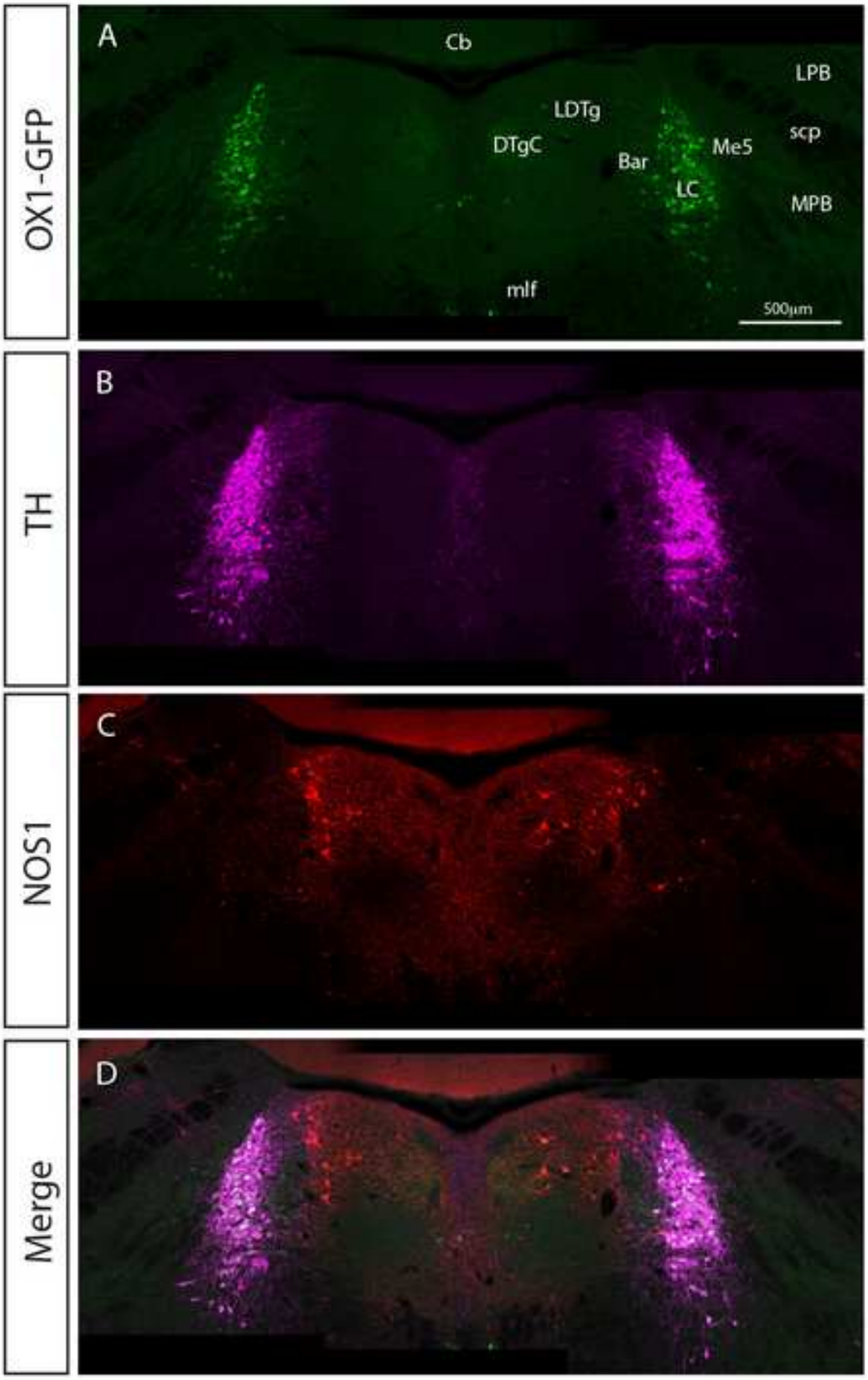

Figure 6

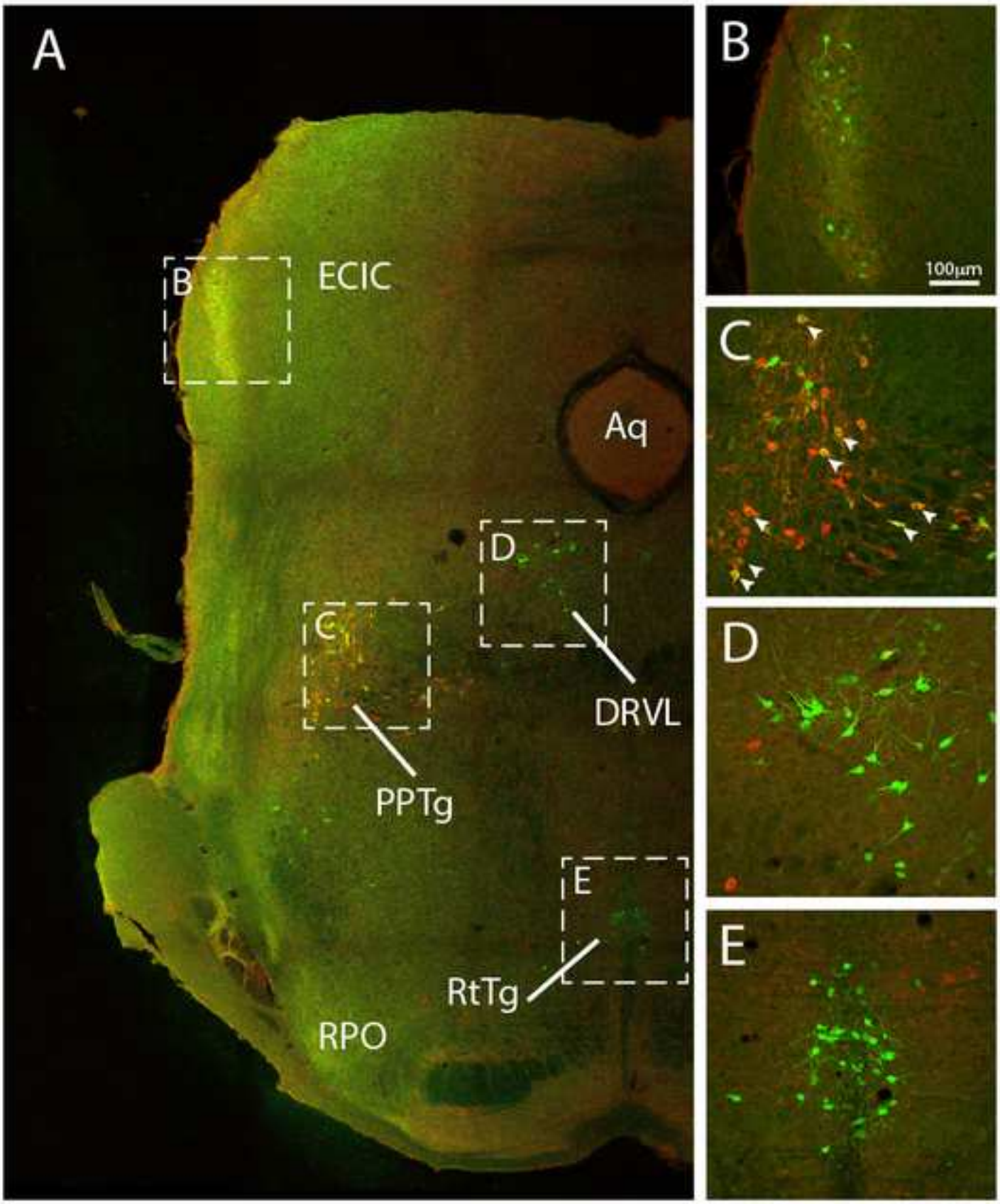

Figure 7